RESEARCH ARTICLE

Key Points:
- In the NE Atlantic, DIC has increased at all depths in the period 1981-2013
- AOU, TA, and $\delta^{13}C_{DIC}$ show that approximately 31% of DIC increase is anthropogenic
- Model output confirms that rates of change determined from observations are robust

Supporting Information:
- Texts S1–S6, Figures S1 and S2, Tables S1, S3, and S4, and Table S2 and Data Set S1–S3 Captions
- Table S2
- Data Set S1
- Data Set S2
- Data Set S3

Correspondence to:
M. P. Humphreys,
m.p.humphreys@soton.ac.uk

Multidecadal accumulation of anthropogenic and remineralized dissolved inorganic carbon along the Extended Ellett Line in the northeast Atlantic Ocean

Matthew P. Humphreys[1], Alex M. Griffiths[2], Eric P. Achterberg[1,3], N. Penny Holliday[4], Victoire M. C. Rérolle[5], Jan-Lukas Menzel Barraqueta[3], Matthew P. Couldrey[1], Kevin I. C. Oliver[1], Susan E. Hartman[4], Mario Esposito[1], and Adrian J. Boyce[6]

[1]Ocean and Earth Science, University of Southampton, Southampton, United Kingdom, [2]Department of Earth Science and Engineering, Imperial College London, London, United Kingdom, [3]GEOMAR Helmholtz Centre for Ocean Research, Kiel, Germany, [4]National Oceanography Centre, Southampton, United Kingdom, [5]Sorbonne Universités (UPMC, University of Paris 06)-CNRS-IRD-MNHN, LOCEAN Laboratory, Paris, France, [6]Scottish Universities Environmental Research Centre, East Kilbride, United Kingdom

Abstract Marine carbonate chemistry measurements have been carried out annually since 2009 during UK research cruises along the Extended Ellett Line (EEL), a hydrographic transect in the northeast Atlantic Ocean. The EEL intersects several water masses that are key to the global thermohaline circulation, and therefore the cruises sample a region in which it is critical to monitor secular physical and biogeochemical changes. We have combined results from these EEL cruises with existing quality-controlled observational data syntheses to produce a hydrographic time series for the EEL from 1981 to 2013. This reveals multidecadal increases in dissolved inorganic carbon (DIC) throughout the water column, with a near-surface maximum rate of $1.80 \pm 0.45\,\mu mol\,kg^{-1}\,yr^{-1}$. Anthropogenic CO_2 accumulation was assessed, using simultaneous changes in apparent oxygen utilization (AOU) and total alkalinity (TA) as proxies for the biogeochemical processes that influence DIC. The stable carbon isotope composition of DIC ($\delta^{13}C_{DIC}$) was also determined and used as an independent test of our method. We calculated a volume-integrated anthropogenic CO_2 accumulation rate of $2.8 \pm 0.4\,mg\,C\,m^{-3}\,yr^{-1}$ along the EEL, which is about double the global mean. The anthropogenic CO_2 component accounts for only $31 \pm 6\%$ of the total DIC increase. The remainder is derived from increased organic matter remineralization, which we attribute to the lateral redistribution of water masses that accompanies subpolar gyre contraction. Output from a general circulation ecosystem model demonstrates that spatiotemporal heterogeneity in the observations has not significantly biased our multidecadal rate of change calculations and indicates that the EEL observations have been tracking distal changes in the surrounding North Atlantic and Nordic Seas.

1. Introduction

Emissions of carbon dioxide (CO_2) from human activities have increased the atmospheric partial pressure of CO_2 (pCO_2), in particular during the last 200 years [*Ahn et al.*, 2012]. This increase, and its well-documented implications for global climate [*International Panel on Climate Change*, 2013], would have been significantly greater without CO_2 uptake by the ocean, which currently sequesters about a quarter of anthropogenic CO_2 emissions each year [*Le Quéré et al.*, 2009]. Ocean CO_2 uptake also induces decline in ocean pH, commonly known as ocean acidification, which will persist for centuries after anthropogenic CO_2 emissions cease [*Caldeira and Wickett*, 2003]. Ocean acidification will have repercussions for marine ecosystems and biogeochemistry that we have only recently begun to understand [*Doney et al.*, 2009; *Gaylord et al.*, 2015].

Open ocean time series sites that monitor marine carbonate chemistry provide essential observational data to quantify long-term trends in anthropogenic CO_2 uptake and acidification [e.g. *Dore et al.*, 2009; *Olafsson et al.*, 2009; *González-Dávila et al.*, 2010; *Bates et al.*, 2012]. The time series data are also used to validate output from global coupled ocean-atmosphere models [*Le Quéré et al.*, 2010]. However, only a handful of these sites exist globally [*Bates et al.*, 2014]. We present a new time series of marine carbonate chemistry measurements for the Extended Ellett Line (EEL), an open ocean transect in the northeast Atlantic Ocean. The EEL runs from Iceland to Scotland via the Rockall Plateau (Figure 1), and repeated physical measurements have been carried out on parts of it since 1975 [*Holliday and Cunningham*, 2013]. The transect captures the flow of warm, salty water
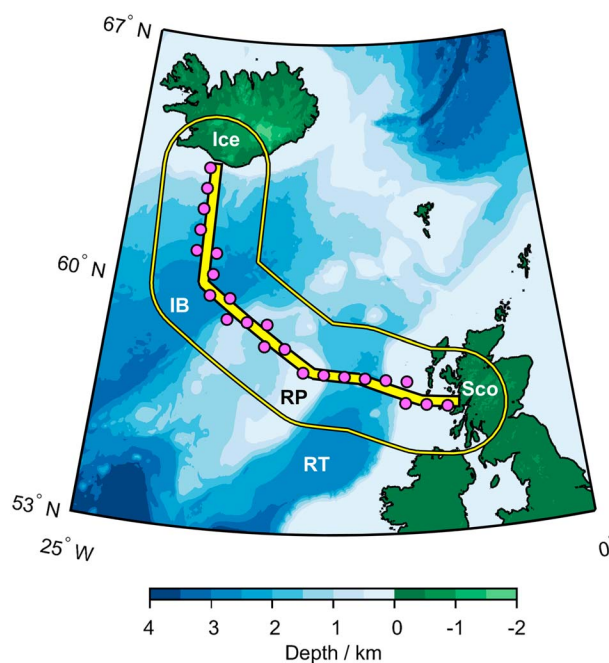
Figure 1. Bathymetric map of the subpolar North Atlantic Ocean, including the idealized EEL route (thick yellow line, Table S1). The thin yellow line shows the 167 km radius zone encompassing the observational data used in this study. The magenta circles show locations of the model stations selected to represent the ideal EEL (i.e., the TAA data set). Abbreviations: IB = Iceland Basin; RP = Rockall Plateau; RT = Rockall Trough; Ice = Iceland; Sco = Scotland.

from the North Atlantic into the Nordic Seas and around half of the returning deep, cold overflow current. The remaining overflow returns south via the west of Iceland [*Hansen and Østerhus*, 2000]. The North Atlantic is an important region to monitor because of its global importance for oceanic uptake and accumulation of anthropogenic CO_2, accounting for about 23% of global oceanic anthropogenic CO_2 storage despite covering only 15% of the global ocean surface area [*Sabine et al.*, 2004; *Khatiwala et al.*, 2009, 2013]. As the EEL will continue to be surveyed by UK research vessels, our analysis provides a baseline within this critical region that can be extended in future years.

Our time series consists of measurements carried out during annual EEL cruises from 2009 to 2013, augmented by hydrographic data from several quality-controlled compilations [*Key et al.*, 2004, 2010; *Schmittner et al.*, 2013]. We have quantified the rate of change of dissolved inorganic carbon (DIC) throughout the water column along the EEL and used simultaneous changes in apparent oxygen utilization (AOU) and total alkalinity (TA) to quantify its anthropogenic (DIC_{anth}) and biogeochemical components. The approach that we have taken to partition the changes in total DIC into these components is based on the same principles as established back-calculation methods for estimating DIC_{anth} [*Brewer*, 1978; *Chen and Millero*, 1979; *Gruber et al.*, 1996]. However, we have determined the relative accumulation of DIC_{anth} during the observational time period (i.e., 1981 to 2013), rather than seeking to evaluate the total DIC_{anth} increase since preindustrial times. This avoids the necessity to estimate preindustrial fields for DIC, AOU, TA and other variables, which is a key source of uncertainty in back-calculation methods [*Matsumoto and Gruber*, 2005; *Sabine and Tanhua*, 2010]. The extended multilinear regression (eMLR) technique is an alternative way to evaluate relative changes in DIC_{anth} [e.g., *Friis et al.*, 2005; *Tanhua et al.*, 2007], but it does not provide information about nonanthropogenic changes in DIC, which we find to be significant at the EEL. The eMLR technique may also be inappropriate due to our study's multidecadal duration [*Goodkin et al.*, 2011]. We have instead determined multidecadal rates of change of the relevant hydrographic variables with linear regressions using all of the data, thereby producing results that are not strongly biased by any individual cruise. These regressions were carried out on constant potential density surfaces, in order to track water masses between cruises [*Pérez et al.*, 2010; *Wanninkhof et al.*, 2010]. Observations of the stable carbon isotopic composition of DIC ($\delta^{13}C_{DIC}$) provided independent support for our deconvolution of the changes in DIC, again through regression-derived rates of change and a process-based approach. Finally, using output from a coupled ocean general circulation biogeochemical model [*Yool et al.*, 2013a], we demonstrated that the calculated rates of change along the EEL do not appear to be biased by the spatiotemporal heterogeneity of the observations and track equivalent changes in the surrounding North Atlantic and Nordic Seas. The model study emphasizes the importance of the EEL for continued future monitoring.

2. Data

2.1. Observations

2.1.1. Recent EEL Cruises

The EEL was occupied annually from 2009 to 2013 by RRS *Discovery* cruises D340 [*Sherwin*, 2009], D351 [*Read*, 2010], D365 [*Read*, 2011] and D379 [*Griffiths*, 2012], and RRS *James Cook* cruise JC086

[*Griffiths and Holliday*, 2013]. During these cruises, seawater samples for DIC and TA were collected and measured as described in the supporting information (Text S1), and conductivity-temperature-depth sensor measurements of temperature, practical salinity, and dissolved oxygen (DO) were carried out and calibrated using manual measurements of discrete samples (Text S2). During cruise D379, samples were also collected to measure $\delta^{13}C_{DIC}$ (Text S3), as detailed by *Humphreys et al.* [2015]. The distributions of these variables from cruise D379 are illustrated in the supporting information (Figure S1).

2.1.2. Syntheses
Data from the GLobal Ocean Data Analysis Project (GLODAP) [*Key et al.*, 2004] and CARbon dioxide IN the Atlantic Ocean (CARINA) [*Key et al.*, 2010] syntheses were combined with the measurements undertaken during the recent EEL occupations. Carbonate chemistry data in GLODAP from the Transient Tracers in the Ocean-North Atlantic Study [*Brewer et al.*, 1985] were adjusted following *Tanhua and Wallace* [2005].

The $\delta^{13}C_{DIC}$ data in GLODAP and CARINA [*Key et al.*, 2004, 2010] have not undergone a secondary quality control process, so we instead used the compilation prepared by *Schmittner et al.* [2013]. This consists of a high-quality subset of the GLODAP and CARINA results, augmented by data from additional cruises [*Gruber et al.*, 1999]. The estimated accuracy of these $\delta^{13}C_{DIC}$ values is between 0.1 and 0.2‰ [*Schmittner et al.*, 2013].

2.1.3. Bathymetry
Bathymetric data from the GEBCO_2014 30 arc second grid (version 20141103, http://www.gebco.net) were obtained for the EEL and its immediate surrounding area. The bathymetry of the idealized EEL route (Table S1) was derived from this data by linear interpolation of depth from the GEBCO_2014 latitude and longitude grids.

2.2. Model Output

We obtained the output of a simulation described in detail by *Yool et al.* [2013a] (referred to as the "anthropogenic simulation"). This had been run from the year 1860 to 2100 and consisted of the size-based intermediate complexity ecosystem model MEDUSA-2.0 [*Yool et al.*, 2013b] coupled to the physical model version 3.2 of the Nucleus for European Modelling of the Ocean (NEMO) [*Madec*, 2008]. The horizontal resolution is approximately $1° \times 1°$ (with 292×362 grid points), and vertical space is divided into 64 levels that increase in thickness from about 6 m at the surface to 250 m at a depth of 6 km. We refer to each vertical column of grid points as a "model station." Surface forcing of NEMO used output from the HadGEM2-ES Earth-system model [*Collins et al.*, 2011], and the DIC and TA fields in MEDUSA-2.0 were initialized using the GLODAP climatology [*Key et al.*, 2004]. Atmospheric pCO$_2$ followed historical data from 1860 to 2005 and then switched to representative concentration pathway 8.5 [*Riahi et al.*, 2011] for the rest of the simulation. We also obtained output from a second "control simulation," which had the same setup except that the mean atmospheric pCO$_2$ was held constant at a preindustrial value of 286 μatm throughout.

3. Methods

3.1. Subsampling

3.1.1. Observations
An "observational" data set (Table S2) was created using all data in GLODAP, CARINA, and from the recent EEL cruises from within 167 km of an idealized EEL route (Figure 1). The route runs in straight lines (great circles, Figure 1) through the waypoints listed in Table S1. Many of the cruises in GLODAP and CARINA passing through the EEL region did not follow the EEL route, so 167 km was chosen as the optimal radius to satisfy the trade-off between capturing sufficient historical data to perform an effective analysis while remaining local to the EEL. Essentially, 167 km was the smallest possible distance that included enough historical data from the earliest time points (in 1981) to perform a robust analysis. The same processing was carried out separately for the *Schmittner et al.* [2013] data set plus the D379 $\delta^{13}C_{DIC}$ measurements [*Humphreys et al.*, 2015], to create the "isotopes" data set (Table S3).

3.1.2. Model Output
The model outputs were subsampled into several different data sets (Table 1). First, monthly mean fields from both simulations (anthropogenic and control) were subsampled to match the spatiotemporal distribution of observational data as closely as possible, using a nearest-neighbor approach. These data sets are hereafter referred to as "Subsampled Anthropogenic Monthly" and "Subsampled Control Monthly"

Table 1. Model Data Sets and Their Abbreviations

Data Set Abbreviation	Dates Included	Locations Included	Simulation	Temporal Resolution
SAM (Subsampled Anthropogenic Monthly)	Matching observations	Matching observations	Anthropogenic	Monthly
SCM (Subsampled Control Monthly)	Matching observations	Matching observations	Control	Monthly
FAA (Full Anthropogenic Annual)	1981 to 2013	Full N Atlantic	Anthropogenic	Annual
TAA (Transect Anthropogenic Annual)	1981 to 2013	Model EEL transect (Figure 1)	Anthropogenic	Annual

(SAM and SCM, respectively). The SAM data set is therefore the model equivalent of the real EEL observations, and SCM is the same but with no anthropogenic CO_2. Second, annual mean fields from the anthropogenic simulation, from 1981 to 2013 inclusive and within the region from 25°N to 75°N and 70°W to 10°E, were extracted to form the "Full Anthropogenic Annual" data set (FAA). Finally, all output at the closest model locations to the idealized EEL transect route (Figure 1) was selected from FAA to form the "Transect Anthropogenic Annual" data set (TAA). This TAA data set can be considered to represent the EEL as if it had been sampled perfectly throughout the study period. The rates of change of variables calculated using TAA are therefore the standard against which the quality of the other model data sets are judged.

3.2. Derived Variables

The potential density anomaly at pressure $(P) = 0$ dbar (σ_0), in situ density (ρ), and potential temperature (θ) were calculated from T, S, and P using the Gibbs-SeaWater Oceanographic Toolbox for MATLAB® (MathWorks®, USA) [*McDougall and Barker*, 2011]. Apparent oxygen utilization (AOU) was calculated from θ, S, and DO using the combined fit coefficients of *García and Gordon* [1992]. The Revelle factor was calculated from DIC, TA, T, S, and P in the surface ocean, assuming negligible silicate and phosphate concentrations, using version 1.1 of the CO_2SYS program for MATLAB [*van Heuven et al.*, 2011], the carbonic acid dissociation constants of *Lueker et al.* [2000], and the boron:chlorinity of *Lee et al.* [2010].

3.3. Interpolations

At each sampling station in each data set, DIC, TA, AOU, S, $\delta^{13}C_{DIC}$, and depth were interpolated to σ_0 values ascending in units of 0.001 from 26 to 28 kg m^{-3} (called "σ_0 levels"), using piecewise cubic Hermite interpolating polynomial (PCHIP) fits to the observations (e.g., Figures 2a–2c) [*Fritsch and Carlson*, 1980; *Kahaner et al.*, 1988]. This was in order to compare these variables between cruises. Potential density is a better interpolant than depth in this context, because it tracks any vertical movements of water masses in the time between successive observations. A small number of stations had fewer than the four unique measurements required to carry out the interpolation, so the measured values were instead assigned directly to their closest σ_0 levels. No extrapolations were performed beyond the measured σ_0 range at any station.

3.4. Rates of Change

For the observational, SAM, SCM, and TAA data sets, ordinary least squares regressions between each variable, and the sampling date across all sampling stations were used to determine the rate of change at each σ_0 level (e.g., Figures 2d–2f). The mean value of each variable was also calculated for each σ_0, again across all sampling stations. We report the rate of change of a variable X at any given σ_0 as $dX/dt = R \pm U$, where R is the rate of change of X and U is its 1σ uncertainty taking into account any autocorrelation in X. These calculations were carried out using the MATLAB® function "regress2" written by I. Eisenmann (Scripps Institution of Oceanography, USA). Rates of change calculated for σ_0 levels that did not include any data from both the earliest and most recent years of data (1992 and 2012, respectively, for $\delta^{13}C_{DIC}$, 1981 and 2012 for DO, and 1981 and 2013 for DIC and TA) were excluded from further analysis.

For the FAA data set, the rates of change were calculated separately at each model station. At each σ_0 level, the rate of change of each variable in the TAA data set was then subtracted from the corresponding FAA rate. These values are reported as $\Delta dX/dt$, and positive values indicate a greater rate in FAA than TAA. Rates of change considered representative of the North Atlantic and Nordic Seas for each σ_0 layer were calculated for each variable by obtaining the mean rate of change at all model stations in the range from 25 to 40°N and 070 to 030°W for the North Atlantic, and 66 to 72°N and 012°W to 001°E for the Nordic Seas.
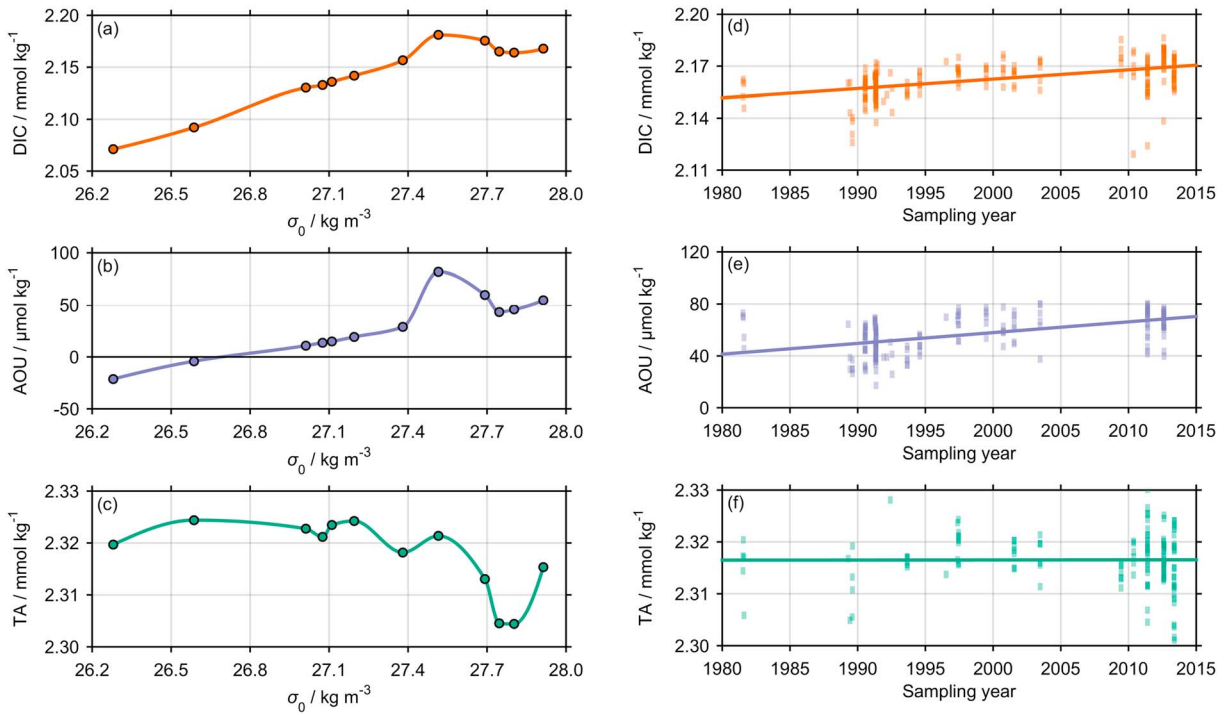
Figure 2. (a–c) Illustration of the PCHIP interpolations used to calculate rates of change for (Figure 2a) DIC, (Figure 2b) AOU, and (Figure 2c) TA, for a typical sampling station (specifically EEL cruise D379, station B12, 12 August 2012). (d–f) Data interpolated to $\sigma_0 = 27.600$ kg m^{-3}, with regression lines showing rates of change: (Figure 2d) DIC, 0.54 ± 0.06 µmol kg^{-1} yr^{-1}, $r = 0.497$, $n = 228$; (Figure 2e) AOU, 0.83 ± 0.10 µmol kg^{-1} yr^{-1}, $r = 0.533$, $n = 188$; (Figure 2f) TA, 0.00 ± 0.05 µmol kg^{-1} yr^{-1}, $r = 0.003$, $n = 132$, where r is the correlation coefficient and n is the number of measurements.

3.5. Components of DIC Change

3.5.1. Using TA and AOU

We can use changes in other observed variables to deconvolve the total DIC change into its component drivers—the carbonate pump (DIC_{carb}), soft tissue pump (DIC_{soft}), and the solubility pump (DIC_{sol}) [*Gruber et al.*, 1996]:

$$dDIC/dt = dDIC_{carb}/dt + dDIC_{soft}/dt + dDIC_{sol}/dt \qquad (1)$$

The "carbonate pump" is the formation and dissolution of calcium carbonate ($CaCO_3$). Increasing its rate of dissolution relative to formation at a given point drives an increase in DIC, accompanied by an increase in TA of double the magnitude [*Wolf-Gladrow et al.*, 2007]. We can therefore determine its contribution to the total $dDIC/dt$ as

$$dDIC_{carb}/dt = 0.5 \cdot \left(dTA/dt - R_{N/O2} \cdot dAOU/dt\right) \qquad (2)$$

where the $dAOU/dt$ term corrects for changes in TA driven by nitrate release during organic matter remineralization and $R_{N/O2}$ is -0.0941 ± 0.0081 [*Anderson and Sarmiento*, 1994].

Biological activity, concentrated near the ocean surface, converts dissolved inorganic nutrients to particulate organic matter (POM), some of which sinks and remineralizes at depth, returning the nutrients to solution: the soft tissue pump. Remineralization also takes up DO, thereby increasing AOU. The component of $dDIC/dt$ caused by changes in organic matter remineralization can therefore be predicted from $dAOU/dt$:

$$dDIC_{soft}/dt = -R_{C/O2} \cdot dAOU/dt \qquad (3)$$

where $R_{C/O2}$ is the increase in DIC as a fraction of DO consumption during this process, which we assume takes a constant value of -0.688 ± 0.092 [*Anderson and Sarmiento*, 1994]. The remaining DIC increase is attributed to increases in air-to-sea CO_2 transfer at the surface outcrop regions for these σ_0 levels. Assuming no significant long-term trend in air-sea pCO_2 disequilibrium from 1981 to 2013 in the

ventilation regions (i.e., $dDIC_{diseq}/dt = 0$), this increase represents the accumulation of anthropogenic DIC (DIC_{anth}):

$$dDIC_{anth}/dt = dDIC_{sol}/dt - dDIC_{diseq}/dt \approx dDIC_{sol}/dt \qquad (4)$$

3.5.2. Using DIC Stable Isotopes

We can relate $d\delta^{13}C_{DIC}/dt$ to changes in the other variables in order to independently test our attribution of $dDIC/dt$ to its components. At each σ_0 level, the total change in $\delta^{13}C_{DIC}$ from 1981 to 2013 ($\Delta\delta^{13}C_{DIC}$) is the sum of the changes caused by the same components that drove the total changes in DIC:

$$\Delta\delta^{13}C_{DIC} = \Delta\delta_{anth} + \Delta\delta_{soft} + \Delta\delta_{carb} \qquad (5)$$

Formation and dissolution of $CaCO_3$ minerals does not cause any significant fractionation of carbon isotopes [*Romanek et al.*, 1992; *Lynch-Stieglitz et al.*, 1995; *Gruber et al.*, 1999], so the $\Delta\delta_{carb}$ term is set to 0. The $\Delta\delta_{anth}$ can be calculated from the total changes in DIC (ΔDIC) and AOU (ΔAOU), and the ratio between anthropogenic changes in $\delta^{13}C_{DIC}$ and DIC (called ΔRC following, e.g., *McNeil et al.* [2001]):

$$\Delta\delta_{anth} = \Delta RC \cdot \left(\Delta DIC + \Delta AOU \cdot R_{C/O2} \right) \qquad (6)$$

The remineralization component $\Delta\delta_{soft}$ also depends on the initial DIC and $\delta^{13}C_{DIC}$ (DIC_i and δ_i respectively), and the isotopic composition of particulate organic carbon POC ($\delta^{13}C_{POC}$):

$$\Delta\delta_{soft} = -\delta_i + \frac{DIC_i \cdot \delta_i - \delta^{13}C_{POC} \cdot \Delta AOU \cdot R_{C/O2}}{DIC_i + \Delta DIC} \qquad (7)$$

The values of the rate of change regression lines for DIC and $\delta^{13}C_{DIC}$ at the midpoint of the year 1981 were used for DIC_i and δ_i. For any variable X, conversion between ΔX and its rate of change is straightforward for the 32 year observational period:

$$\Delta X = 32 \cdot dX/dt \qquad (8)$$

Combining (6) and (7) into (5) and rearranging, we obtained the following relationship for each σ_0 level:

$$\Delta\delta^{13}C_{DIC} = \Delta RC \left(\Delta DIC + \Delta AOU \cdot R_{C/O2} \right) - \delta^{13}C_{POC} \left(\frac{\Delta AOU \cdot R_{C/O2}}{DIC_i + \Delta DIC} \right) - \delta_i + \frac{DIC_i \cdot \delta_i}{DIC_i + \Delta DIC} \qquad (9)$$

Considering the terms $\Delta\delta^{13}C_{DIC}$, δ_i, DIC_i, ΔDIC, and ΔAOU to represent column vectors in which each row corresponds to a different σ_0 level, and ΔRC and $\delta^{13}C_{POC}$ as unknown scalar constants, (9) was further rearranged and rewritten in matrix form:

$$\left[(\mathbf{DIC_i} + \mathbf{\Delta DIC}) \circ \left(\mathbf{\Delta DIC} + \mathbf{\Delta AOU}\, R_{C/O2} \right) \quad -\mathbf{\Delta AOU}\, R_{C/O2} \right] \begin{bmatrix} \Delta RC \\ \delta^{13}C_{POC} \end{bmatrix}$$
$$= (\mathbf{DIC_i} + \mathbf{\Delta DIC}) \circ \left(\mathbf{\Delta\delta^{13}C_{DIC}} + \mathbf{\delta_i} \right) - \mathbf{DIC_i} \circ \mathbf{\delta_i} \qquad (10)$$

where the open circle symbols denote the Hadamard (element-wise) product. For the system of linear equations thus generated, the least squares best solution for ΔRC and $\delta^{13}C_{POC}$ across all σ_0 levels was then determined. The 95% bootstrap confidence intervals for ΔRC and $\delta^{13}C_{POC}$ were calculated using the bias corrected and accelerated percentile method with 10^4 bootstrap resamples.

3.6. Column Inventories

To volume integrate the rates of change for each variable, we first calculated the average depth of each σ_0 level and determined its lateral extent using the GEBCO_2014 bathymetric grid. The column inventories were then determined from the σ_0 depths, widths, and rates of change. The approach is described in detail in the supporting information (Text S5).

4. Results and Discussion

4.1. Multidecadal DIC Increase

4.1.1. Water Column Changes in the Observations

We observe increases in DIC from 1981 to 2013 throughout the water column. The maximum $dDIC/dt$ of $1.80 \pm 0.45\ \mu mol\ kg^{-1}\ yr^{-1}$ is found in the upper 30 m of the water column ($\sigma_0 \approx 26.7\ kg\ m^{-3}$, Figures 3a and 4a).
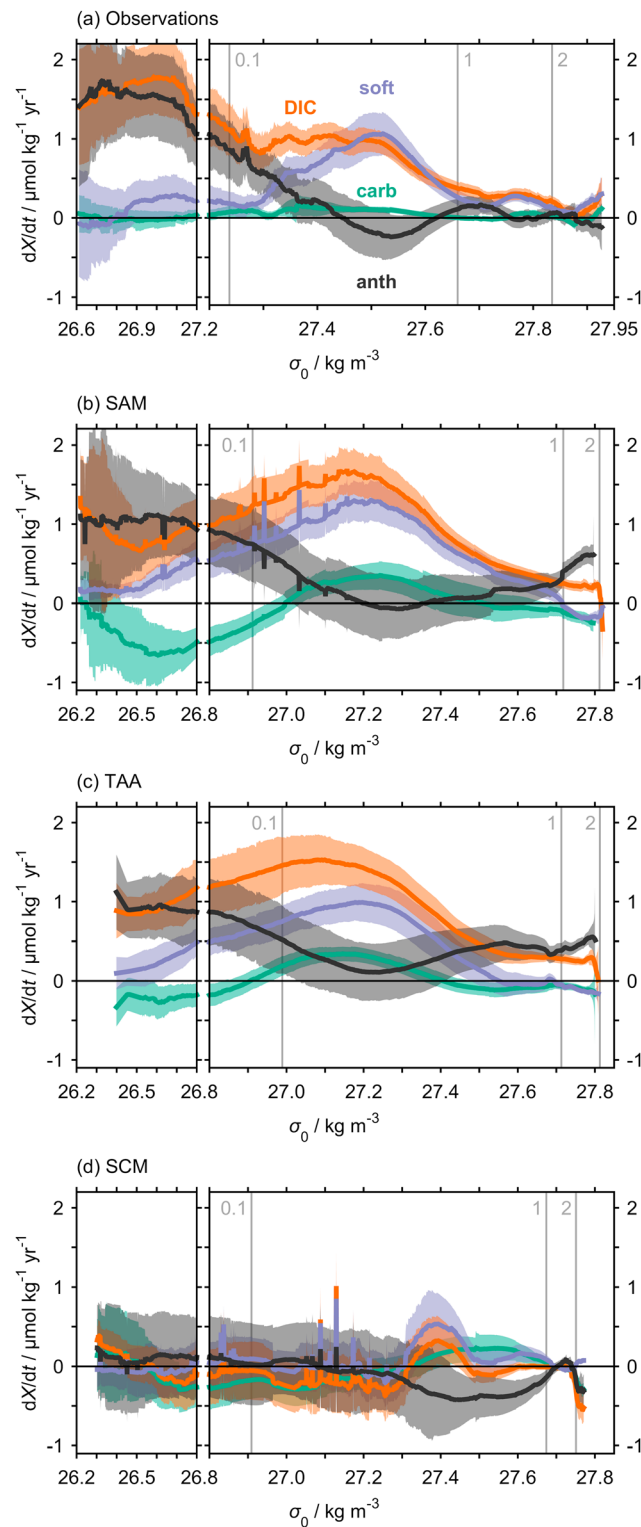
Figure 3. Multidecadal rates of change of dissolved inorganic carbon (DIC) and its components DIC_{soft}, DIC_{carb}, and DIC_{anth} (in orange, violet, green, and black, respectively) throughout the water column for the (a) observational, (b) SAM, (c) TAA, and (d) SCM data sets (Table 1). The shaded regions indicate ± uncertainty. The vertical grey lines are at σ_0 levels with mean depths of 0.1, 1, and 2 km in each data set, as labeled. Note the different horizontal axis scale for Figure 3a.

This corresponds to an increase in seawater pCO_2 of about 3.6 µatm yr^{-1} (calculated from the mean Revelle factor for this σ_0 layer). This is greater than the atmospheric pCO_2 increase rate of about 1.6 µatm yr^{-1} [*Tjiputra et al.*, 2014], which supports some previous studies that suggest that the oceanic sink for atmospheric CO_2 has been decreasing in this region [e.g., *Schuster et al.*, 2009]. Below the surface layer, dDIC/dt decreases to a deep minimum of 0.02 ± 0.10 µmol kg^{-1} yr^{-1} ($\sigma_0 \approx 27.9$ kg m^{-3}, approximately 2 km and deeper, Figures 3a and 4a). The non-zero dDIC/dt means that the carbonate, soft tissue, and solubility pump processes controlling DIC [*Gruber et al.*, 1996] are not operating in a steady state.

Changes in TA in the observations are very small: dTA/dt is between 0.23 ± 0.26 and -0.19 ± 0.10 µmol kg^{-1} yr^{-1}, and consequently, $dDIC_{carb}$/dt is in the range between 0.16 ± 0.13 and -0.09 ± 0.05 µmol kg^{-1} yr^{-1} (Figures 3a and 4b). Therefore, the observed DIC increase was not significantly driven by changes in the carbonate pump.

Changes in AOU are also virtually zero near the surface, but there have been increases in AOU deeper in the water column. As a result, $dDIC_{soft}$/dt closely tracks dDIC/dt for $\sigma_0 > 27.45$ kg m^{-3} (Figures 3a and 4c). This component of dDIC/dt can be attributed to a multidecadal increase in the amount of remineralized organic matter at these σ_0 levels. Two possible mechanisms could explain this phenomenon.

First, there could have been an increase in export and remineralization of POM at the EEL itself. The indirect evidence does not support this hypothesis. Although there have not been sufficient observations to directly confirm the presence or absence of a multidecadal trend in POM export and remineralization in the EEL region, POM export is unlikely to be increasing fast enough to cause the observed pattern in $dDIC_{soft}$/dt (as derived from dAOU/dt). Export rates can be estimated as a function of surface chlorophyll a, with higher concentrations

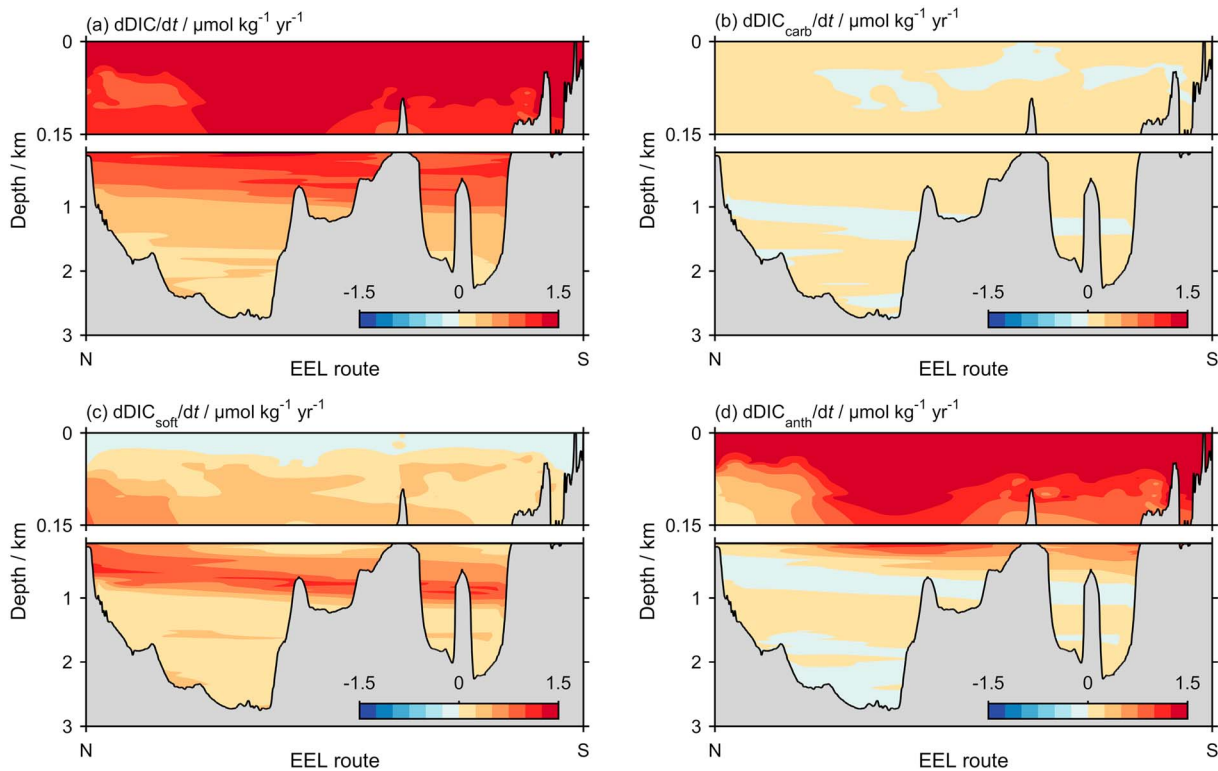**Figure 4.** Multidecadal rates of change of (a) DIC, and its components (b) DIC_{carb}, (c) DIC_{soft}, and (d) DIC_{anth}, mapped onto the σ_0 field observed by cruise D379 in August 2012 (supporting information Figure S1h).

accompanying higher export rates [e.g., *Dunne et al.*, 2007]. However, satellite observations have detected a small decline in chlorophyll *a* from 1998 to 2012 for the northern North Atlantic [*Gregg and Rousseaux*, 2014], which is inconsistent with increasing in situ POM export.

Alternatively, there could have been changes in the lateral distribution of water masses along isopycnals, bringing waters with higher AOU (more remineralized POM) into the EEL region. At σ_0 levels lighter than about 27.7 kg m^{-3}, the EEL samples a mixture of waters from the subtropical and subpolar gyres. Contraction of the subpolar gyre increases the subtropical component, while expansion decreases it. The subpolar gyre index (SPGI) metric can be interpreted as a measure of subpolar gyre contraction, with lower values indicating a more contracted gyre [*Hátún et al.*, 2005]. Overall, there has been a decrease in the SPGI during the period of our study, especially since the early 1990s [*Häkkinen and Rhines*, 2004; *Hátún et al.*, 2005; *Hughes et al.*, 2012]. This phenomenon has separately been shown to drive declining macronutrient concentrations in the Rockall Trough [*Johnson et al.*, 2013]. The subtropical waters influencing the EEL in this way are a combination of Eastern North Atlantic Water, formed in the Bay of Biscay [*McGrath et al.*, 2012a], and highly saline Mediterranean water [*Burkholder and Lozier*, 2011; *McGrath et al.*, 2012a]. Data from GLODAP and CARINA [*Key et al.*, 2004, 2010] indicate that, to first order, DIC and AOU increase to the south of the EEL region along σ_0 levels in these water masses. An increasing southern influence on the water at the EEL would therefore be expected to increase DIC and AOU at the EEL, like we observe.

The remaining DIC increase is interpreted as anthropogenic and is confined in and above the thermocline ($\sigma_0 < 27.5$ kg m^{-3}, Figures 3a and 4d). This matches previous global-scale studies of the DIC_{anth} and anthropogenic tracer distributions [e.g., *Sabine et al.*, 2004]. In this upper part of the water column, our calculated $dDIC_{anth}/dt$ is consistent with similar analyses in the nearby or overlapping regions of the Iceland Basin [*Pérez et al.*, 2010] and southern Rockall Trough [*McGrath et al.*, 2012b]. At greater depths, $dDIC_{anth}/dt$ is virtually zero.

Between a σ_0 of 27.70 and 27.85 kg m^{-3}, the EEL samples Labrador Sea Water (LSW). In the EEL region, the properties of LSW are highly variable both spatially and temporally. This is because LSW undergoes extensive mixing with other water masses, including recirculating LSW ventilated in earlier years, during its transport

from the Labrador Sea to the northeast Atlantic [*Yashayaev et al.*, 2007]. So, although we do not observe an increase in DIC_{anth} in the LSW during the study period, any anthropogenic signal from the source region could have been suppressed by mixing. However, we observed a small positive $dDIC/dt$ in LSW ($\sim 0.3\ \mu mol\ kg^{-1}\ yr^{-1}$). It is unlikely that this was caused by increased in situ remineralization, not only for the reasons already described for waters nearer the surface but also because virtually all POM that is generated in the EEL region is remineralized within the mesopelagic zone, which is shallower than the LSW [*Henson et al.*, 2012]. Other studies have identified increases in LSW DIC_{anth} during time periods and within regions that were similar, but crucially not identical, to those considered here [*Pérez et al.*, 2010; *McGrath et al.*, 2012b]. The $dDIC_{anth}/dt$ discrepancy is likely to be an artifact of differences between studies in the distribution of observations of this highly variable water mass.

We do not observe any DIC_{anth} accumulation in the water masses below the LSW, in the deepest part of the water column ($\sigma_0 > 27.85\ kg\ m^{-3}$), although there are small increases in DIC and DIC_{soft} (Figure 3a). These waters, like the LSW, have been significantly altered by mixing since their formation in the Nordic Seas and subsequent flow through one of several narrow channels over the Greenland-Scotland ridge and into the EEL region [*Hansen and Østerhus*, 2000]. This prevents us from directly attributing the DIC and AOU increases to a specific driver.

4.1.2. Choice of POM Stoichiometry

The choice of POM stoichiometry controls the values of $R_{C/O2}$ and $R_{N/O2}$, which clearly influences our partitioning of $dDIC/dt$ into its carbonate (2) and soft tissue components (3). We selected values for $R_{C/O2}$ and $R_{N/O2}$ of -0.688 ± 0.092 and -0.0941 ± 0.0081, respectively, which are based on global macronutrient measurements [*Anderson and Sarmiento*, 1994]. These feature a higher O_2 coefficient than the "original" stoichiometry of *Redfield et al.* [1963], which gives -0.768 for $R_{C/O2}$ and -0.116 for $R_{N/O2}$. This higher O_2 coefficient is supported by considerations of the composition of several groups of algal biomolecules [*Anderson*, 1995]. Although switching between these stoichiometries does create a systematic offset in the results, the size of this offset is no larger than the random uncertainty inherent in the calculations. Switching creates a difference of $0.05\ \mu mol\ kg^{-1}\ yr^{-1}$ in the mean $dDIC_{anth}/dt$ across all σ_0 levels, and a difference in the column inventory changes for the entire EEL of about 8%, with the newer stoichiometry [*Anderson and Sarmiento*, 1994] giving a higher DIC_{anth} inventory. For comparison, the random uncertainty propagated into this inventory estimate from the rates of change themselves is about 9% of the mean value. Furthermore, the original value for $R_{C/O2}$ [*Redfield et al.*, 1963], which has a much greater influence on the DIC_{anth} calculation than $R_{N/O2}$ does, falls within the stated uncertainty of the more recent result [*Anderson and Sarmiento*, 1994]. Consequently, we do not consider this choice to be a particularly important source of uncertainty in our final results.

4.1.3. Column Inventories

The global ocean anthropogenic CO_2 sink was about $2\ Pg\ C\ yr^{-1}$ for the period from 1981 to 2013 [*Le Quéré et al.*, 2010], which corresponds to a global mean DIC_{anth} accumulation rate of about $1.5\ mg\ C\ yr^{-1}\ m^{-3}$ [*Eakins and Sharman*, 2010]. For the idealized EEL route, the column inventory $C(dDIC_{anth}/dt)$ is $2.8 \pm 0.4\ mg\ C\ m^{-3}\ yr^{-1}$, which is about double the global average value. The equivalent $C(dDIC/dt)$ is $9.0 \pm 1.0\ mg\ C\ m^{-3}\ yr^{-1}$, so the DIC_{anth} increase accounts for only $31 \pm 6\%$ of the total DIC accumulation. Virtually, all of the remainder is a result of the increased remineralized organic matter, contained in the increased supply of southern sourced waters that have been brought into the region by contraction of the subpolar gyre, as discussed in section 4.1.1.

The EEL region is part of the largest source of DIC into the Nordic Seas through advection of Atlantic waters over the Greenland-Scotland ridge [*Jeansson et al.*, 2011]. Presently, the Nordic Seas are an important sink for anthropogenic CO_2, convectively transporting it from the surface layer into the interior and then returning it back into the deep North Atlantic [*Jutterström et al.*, 2008; *Olsen et al.*, 2010]. Increasing DIC concentrations in the North Atlantic waters prior to their transport over the ridge might therefore hinder the efficiency of the Nordic Seas CO_2 sink, by inhibiting further uptake of atmospheric CO_2 across the air-sea interface. However, the impact of this effect may be limited, as much of the DIC_{anth} transported into the ocean interior in the Nordic Seas arrives in the surface ocean through advection and is not taken up locally by air-sea exchange [*Olsen et al.*, 2006].

Measurements of chlorofluorocarbon (CFC) inventory changes in the North Atlantic have demonstrated that CFC column inventory variability can be dominantly controlled by changes in volume of different water masses
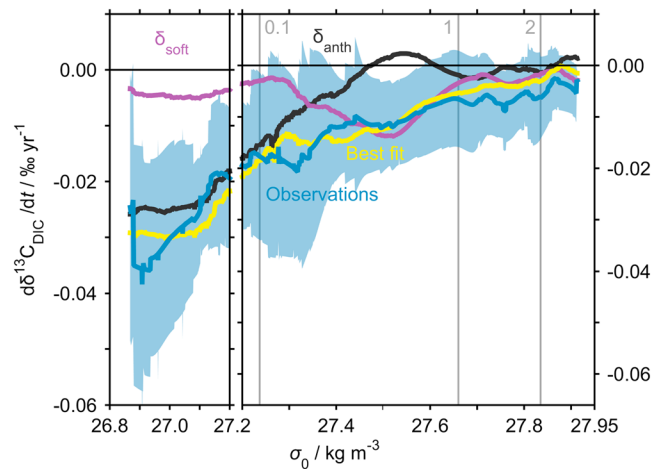
Figure 5. Observed and predicted ("best fit") rate of change of $\delta^{13}C_{DIC}$ for the EEL. Blue line and shading shows rate ± uncertainty evaluated directly from observations; yellow line shows rate predicted from observed $dDIC/dt$ and $dAOU/dt$ using best fit ΔRC and $\delta^{13}C_{POC}$. Note that the prediction is not independent of the observations, but it illustrates the best possible fit. Anthropogenic and remineralized components of the prediction are shown separately (black and purple lines labeled δ_{anth} and δ_{soft} respectively; (5) and (6)). Vertical grey lines indicate σ_0 levels with mean depths of 0.1, 1, and 2 km, as labeled.

at a given location, rather than changes in the CFC concentration within each water mass [*Kieke et al.*, 2007; *Steinfeldt et al.*, 2009]. A similar conclusion has also been suggested for anthropogenic DIC [*Pérez et al.*, 2010]. However, the time scale of volumetric variability in these studies is subdecadal. For our longer, multidecadal study period from 1981 to 2013, we find that changes in σ_0 layer thicknesses are negligible, and their inclusion in the inventory calculations would change the final result by an order of magnitude less than its uncertainty.

4.2. Stable Isotopes of DIC

There are far fewer $\delta^{13}C_{DIC}$ observations than for the other variables, and the length of the time series is shorter, running only from 1993 to 2012. Nevertheless, changes in $\delta^{13}C_{DIC}$ can be used as an independent test of our attribution of the changes in DIC to its anthropogenic and soft tissue components, as these are the two main processes influencing $\delta^{13}C_{DIC}$ in the interior ocean. First, uptake of anthropogenic CO_2 results in a decrease in $\delta^{13}C_{DIC}$, known as the Suess effect, because fossil fuel carbon is isotopically light relative to modern seawater [*Keeling*, 1979]. Second, particulate organic carbon (POC) remineralization also decreases $\delta^{13}C_{DIC}$, because POC has a lighter isotopic signature than typical seawater. According to a meta-analysis study, surface ocean $\delta^{13}C_{POC}$ is between −20 and −30‰ at the latitude and sea surface T of the EEL [*Goericke and Fry*, 1994], compared with typical seawater DIC values near 0‰ [*Olsen and Ninnemann*, 2010; *Schmittner et al.*, 2013; *Humphreys et al.*, 2015]. The carbonate pump does not significantly affect $\delta^{13}C_{DIC}$, because marine carbonate mineral formation (calcification) does not significantly fractionate carbon. Carbonate minerals usually have a $\delta^{13}C$ composition similar to that of the surrounding seawater [*Romanek et al.*, 1992; *Lynch-Stieglitz et al.*, 1995; *Gruber et al.*, 1999].

We observed negative $d\delta^{13}C_{DIC}/dt$ values throughout the water column. The magnitude of $d\delta^{13}C_{DIC}/dt$ decreased from a maximum of $-0.038 \pm 0.026‰\,yr^{-1}$ at near-surface σ_0 levels to a minimum of $-0.002 \pm 0.006‰\,yr^{-1}$ at depth (Figure 5). *Quay et al.* [2007] used a multilinear regression approach to identify a mean $d\delta^{13}C_{DIC}/dt$ of $-0.018 \pm 0.002‰\,yr^{-1}$ for the entire Atlantic Ocean surface mixed layer from 1981 to 2003. They also found that $d\delta^{13}C_{DIC}/dt$ increased to between -0.04 and $-0.05‰\,yr^{-1}$ in the subpolar region between 40°N and 60°N, due to a combination of changes in water mass properties and anthropogenic CO_2 uptake. Their findings are consistent with our near-surface results for the EEL.

We deconvolved the $d\delta^{13}C_{DIC}/dt$ distribution into anthropogenic and remineralized components, which are controlled by the variables ΔRC and $\delta^{13}C_{POC}$. The least squares best fit solutions of (10) for ΔRC and $\delta^{13}C_{POC}$ across all σ_0 levels were $-0.0166 \pm 0.0003‰\,(\mu mol\,kg^{-1})^{-1}$ and $-27.0 \pm 0.5‰$, respectively. To visualize the results, $d\delta^{13}C_{DIC}/dt$ was predicted using (9), with the best fit values of ΔRC and $\delta^{13}C_{POC}$, and the observed rates of $dDIC/dt$ and $dAOU/dt$ (Figure 5). It is inevitable that mean value of the best fit $d\delta^{13}C_{DIC}/dt$ profile will match that of the observations, because of how the ΔRC and $\delta^{13}C_{POC}$ were determined. However, if there were elements of the observed $d\delta^{13}C_{DIC}/dt$ profile that were not driven by DIC_{anth} or DIC_{soft} inputs (e.g., driven by DIC_{carb}), then we would expect the shape of the predicted profile to deviate from the observations in the relevant σ_0 range. This does not occur, and hence, we conclude that DIC_{anth} and DIC_{soft} inputs are indeed the dominant drivers of the observed interior $\delta^{13}C_{DIC}$ changes.

It was originally proposed that ΔRC might take a relatively globally uniform value between -0.016 and $-0.019‰\,(\mu mol\,kg^{-1})^{-1}$ [*Heimann and Maier-Reimer*, 1996]. More recently, it has been demonstrated that

ΔRC can deviate from this global average to exhibit significant spatial variation in certain regions [e.g., *McNeil et al.*, 2001; *Olsen et al.*, 2006], because the air-sea equilibration time is an order of magnitude faster for DIC than for $\delta^{13}C_{DIC}$ [*Lynch-Stieglitz et al.*, 1995]. *Körtzinger et al.* [2003] calculated ΔRC throughout the North Atlantic, reporting a value of -0.022 ± 0.002‰ $(\mu mol\,kg^{-1})^{-1}$ for the σ_0 levels observed in this study, while *Olsen et al.* [2006] found a wide range of ΔRC between about 0.00 and -0.03‰ $(\mu mol\,kg^{-1})^{-1}$ in the upper 100 m of the nearby Nordic Seas. Our best fit value for ΔRC, -0.0166 ± 0.0003‰ $(\mu mol\,kg^{-1})^{-1}$, is at the lower end of, but consistent with, these published results.

We next evaluate our value for $\delta^{13}C_{POC}$ relative to previous estimates in a similar way. Using the linear regression between sea surface T and $\delta^{13}C_{POC}$ proposed by *Goericke and Fry* [1994] (for the northern hemisphere and $T > 5°C$), and a value of 11°C for T (the mean of all EEL T observations for which $P \le 10$ dbar), we would predict $\delta^{13}C_{POC} = -23 \pm 4$‰ for the EEL (we have estimated the uncertainty by eye from the figures presented by *Goericke and Fry* [1994]). Congruently, a more recent global compilation of $\delta^{13}C_{POC}$ results reports $\delta^{13}C_{POC}$ in the approximate range from -18 to -27‰ for the latitude range of the EEL [*Young et al.*, 2013]. Thus, our least squares solution for $\delta^{13}C_{POC}$ of -27.0 ± 0.5‰ is concordant with these and other published values [e.g., *Rau et al.*, 1997].

We conclude that the $d\delta^{13}C_{DIC}/dt$ observations provide independent support for our quantitative attribution of dDIC/dt to anthropogenic and remineralization components.

4.3. Model Output
4.3.1. Subsampled Model Output and Observational Data
Before discussing the rates of change calculated from the model data sets, we first assess how well the distributions of the absolute values of the modeled variables agreed with the observations. For this, we will use the SAM and SCM data sets, which have been subsampled to match the spatiotemporal distribution of the observational data. It is not necessary for these absolute value distributions to be identical in order to compare rates of change between the different data sets. However, if the model distributions were to diverge significantly from the observations for reasons that could not be explained, then the utility of the model as an analogue to the real world would be severely limited. An important caveat is that only one model has been used here, and others might result in different outcomes.

There was no significant systematic offset between the latitude, longitude, and date of the observations and their matching points in the SAM and SCM data sets (Figures 6a–6c). A small fraction of the observations are represented by significantly shallower model data (Figure 6d), due to the coarseness of the model grid relative to the length scale of real-world bathymetric features in this region. However, the overall systematic offset remains insignificant, as the mean difference between observed and matching-model depth was -19 m (shallower in the subsampled model than the observations). This means that the model data sets, which have been spatially and temporally subsampled to "look like" the observations, do so very successfully.

The modeled physical and biogeochemical variables under investigation deviated further from the observations than the spatiotemporal metavariables. The SAM and SCM data sets share very similar σ_0 fields, both offset toward lower values than their matching observations (Figure 6e), especially in the deepest part of the water column. This may be caused by the unrealistic northward penetration of Antarctic Bottom Water (AABW) in the NEMO run used here [*Yool et al.*, 2013a], combined with the model tendency to underestimate the density of this AABW [*Heuzé et al.*, 2013]. The SAM and SCM AOU fields are also very similar to each other, and both represent their matching observations relatively well (Figure 6f). In SAM, DIC takes consistently high values relative to SCM (Figure 6g), so as expected some anthropogenic CO_2 should be detectable in the SAM data set. The DIC in SAM is also consistently high relative to the observations, but the offset is fairly consistent across the entire DIC range, with the fit quality otherwise similar as for AOU. The TA fields from both SAM and SCM diverge considerably from reality, covering a much wider and higher range of values (Figure 6h). However, as they have similar distributions to each other, this should not adversely affect identification of the anthropogenic CO_2 signal in SAM.

In terms of rates of change, SAM does represent the pattern for the observations in the upper water column reasonably well (Figure 3b). Its $dDIC_{anth}/dt$ decreases away from surface, where it takes values close to $1.0\,\mu mol\,kg^{-1}\,yr^{-1}$, to effectively 0 at a σ_0 of about 27.2 kg m^{-3}, in agreement with the observations. The rates dDIC/dt and $dDIC_{soft}/dt$ are similarly well matched. Deeper in the water column, between mean depths

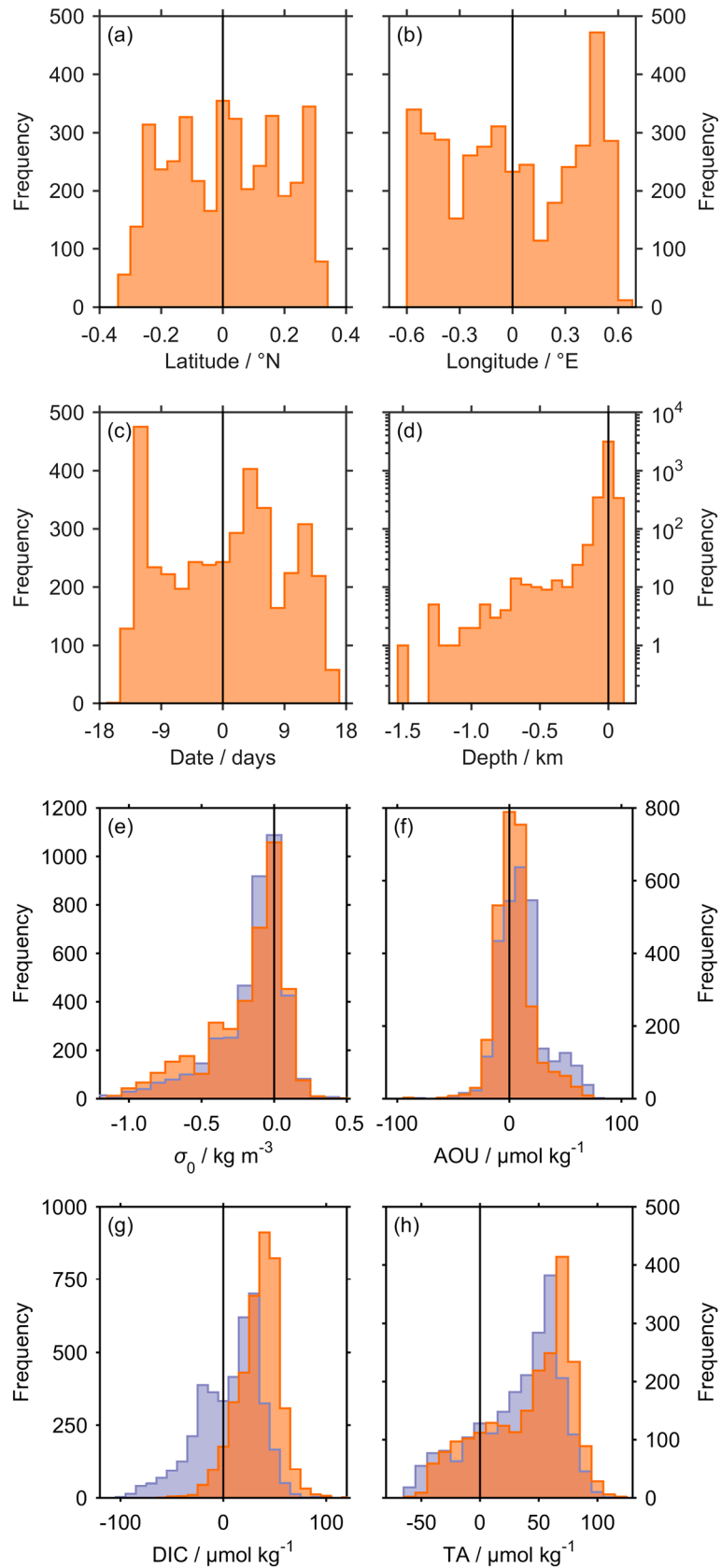**Figure 6.**

of about 1 and 2 km, there is a small increase of about $0.5\,\mu mol\,kg^{-1}\,yr^{-1}$ in DIC_{anth} in SAM. This is absent from the observations; we find a similar pattern in the same depth range for DIC_{anth} in SCM (Figure 3d), indicating that it may be due to model drift in the absence of a long spin-up period. Alternatively, it may be associated with the high northward AABW penetration that we identified as a possible cause of relatively low σ_0 in the models [*Hieronymus and Nycander*, 2013; *Heuzé et al.*, 2014]. Otherwise, SCM does not show significant changes in any of the tested variables, and the patterns with depth appear mostly random. The $dDIC_{carb}/dt$, which is mostly dependent upon dTA/dt (2), exhibits changes in SAM that are absent from the observations throughout the water column. However, like for DIC_{anth} in the deeper part of the water column, we find a similar pattern in SCM, again suggesting that it may result from model drift.

4.3.2. Spatiotemporal Sampling Heterogeneity

The model data sets can be used to estimate the uncertainty introduced into the observational rates of change from spatiotemporal heterogeneity in the data distribution. To do this, we compared the rates of change calculated for the anthropogenic simulation subsampled to match the observations (SAM, Figure 3b) with those from the same simulation but with no missing values (TAA, Figure 3c). The mean ± standard deviation of the differences in rates of change between SAM and TAA across all σ_0 are -0.01 ± 0.14 for DIC, 0.25 ± 0.36 for TA, -0.27 ± 0.18 for AOU, and $+0.06 \pm 0.17$ for DIC_{anth}, all in $\mu mol\,kg^{-1}\,yr^{-1}$. These differences, particularly for DIC_{anth}, are up to an order of magnitude smaller than typical uncertainties in the rates of change themselves, indicating that the spatiotemporal heterogeneity of the observational data distribution has not adversely affected the calculated rates of change for these variables.

4.3.3. Subdecadal Variability

It has been separately shown using observational data that multidecadal trends in DO (and therefore AOU) can be identified despite substantial short-term interannual variability in a shorter, 19 year time series transect close to the EEL, which samples several water masses also present at the EEL [*Stendardo et al.*, 2015]. However, difficulties are presented over shorter time scales, as described below. It has been suggested that a higher rate of DIC_{anth} accumulation can be identified in the Iceland Basin during the high North Atlantic Oscillation (NAO) index period from 1991 to 1998, compared with the lower NAO index (NAOI) period from 1997 to 2006 [*Pérez et al.*, 2010]. The NAOI can be defined in several different ways, all associated with the atmospheric pressure difference between Iceland and the Azores, with a more positive NAOI indicating a greater difference in pressure [*Hurrell et al.*, 2003]. This pressure difference affects the local atmospheric circulation and surface wind speeds and consequently can influence surface ocean currents and air-sea gas exchange [*Thomas et al.*, 2008; *Gruber*, 2009].

To test for any NAOI signal in our data, we calculated $dDIC_{anth}/dt$ using the same methods as for the observational SAM and TAA data sets but restricted to these two shorter date ranges (1991 to 1998 and 1997 to 2006). We find greater $dDIC_{anth}/dt$ for the latter, low-NAOI period in the observations, an opposite result to *Pérez et al.* [2010], although part of their DIC_{anth} increase was due to changing σ_0 layer volumes rather than changes within σ_0 layers. More importantly, our calculated rates are barely distinguishable from uncertainties, because fewer data are available for shorter time periods, so the statistical significance of any apparent nonzero trends is much lower. For the full observational data set (1981 to 2013), the median uncertainty in $dDIC_{anth}/dt$ across all σ_0 is $0.33\,\mu mol\,kg^{-1}\,yr^{-1}$, while the equivalent figures for 1991 to 1998 and 1997 to 2006 are 1.94 and $1.99\,\mu mol\,kg^{-1}\,yr^{-1}$, respectively.

The atmospheric forcing used in the model simulations does not necessarily contain an NAO-like phenomenon, and even if there was one present, it would not be expected to vary simultaneously with the real NAO. This is because the atmospheric data is entirely model generated, rather than being from an atmospheric reanalysis. Consequently, an NAO effect cannot be directly observed in the model data sets. However, the model outputs can be used to indicate the unreliability of rates calculated using the EEL time

Figure 6. Offsets between observations and matching values from the subsampled monthly model outputs (SAM and SCM), for (a) latitude (mean ± SD is $+0.01 \pm 0.18°N$), (b) longitude ($+0.00 \pm 0.37°E$), (c) date (1.3 ± 7.9 days), and (d) depth (-19 ± 117 m). Note logarithmic vertical axis scale for Figure 6d. The distributions for the anthropogenic and control simulations (SAM and SCM, respectively) are identical for these metavariables but are different for the other variables in SAM (orange) and SCM (violet): (e) potential density (SAM mean ± SD is $-0.14 \pm 0.26\,kg\,m^{-3}$, SCM $-0.15 \pm 0.24\,kg\,m^{-3}$), (f) apparent oxygen utilization (SAM $+2.9 \pm 18.7$, SCM $+9.1 \pm 22.4\,\mu mol\,kg^{-1}$), (g) dissolved inorganic carbon (SAM $+38 \pm 18$, SCM $+9 \pm 31\,\mu mol\,kg^{-1}$), and (h) total alkalinity (SAM $+46 \pm 33$, SCM $+32 \pm 38\,\mu mol\,kg^{-1}$).
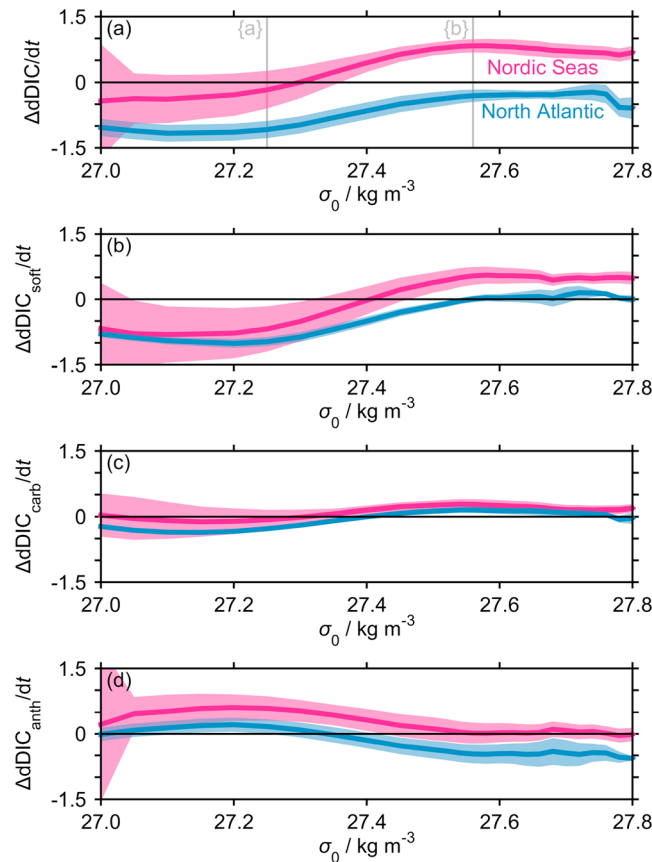
Figure 7. Mean of (a) dDIC/dt and its components (b) dDIC$_{soft}$/dt, (c) dDIC$_{carb}$/dt, and (d) dDIC$_{anth}$/dt in the FAA data set in selected regions, relative to equivalent rate in the ideal model EEL transect data set TAA at the same σ_0 level. Positive values indicate that the faster rate is in the FAA data set. "Nordic Seas" data (pink) is from 66 to 72°N and 012°W to 001°E; "North Atlantic" (blue) is from 25 to 40°N and 070 to 030°W. Shaded areas show ± 2 standard deviations about the mean values. In Figure 7a, the vertical lines marked {a} and {b} indicate the σ_0 levels for Figures 8a and 8b, respectively.

series data for these shorter time periods. The root-mean-square difference between dDIC$_{anth}$/dt in the SCM and TAA data sets is 0.19 µmol kg^{-1} yr^{-1} for 1981 to 2013, but it increases 0.93 µmol kg^{-1} yr^{-1} for 1997 to 2006 and 2.39 µmol kg^{-1} yr^{-1} from 1991 to 1998. The spatiotemporal heterogeneity of the observations therefore does adversely affect the calculated rates of change on these shorter time scales.

That is not to say that the NAO does not influence dDIC/dt and its components. Indeed, we attribute the positive dDIC$_{soft}$/dt to contraction of the subpolar gyre. This was probably itself driven by the NAO, as the atmospheric weather regimes associated with a positive NAOI phase tend to cause northward extension of the North Atlantic subtropical gyre [*Gruber*, 2009; *Barrier et al.*, 2014]. Unfortunately, the significant increase in uncertainty that we find in the rates of change calculated over shorter time scales prevents these data from being used to support a direct link between the NAOI and the water column DIC at these shorter timescales.

In future studies, it may be instructive to investigate relationships between changes in water column DIC beneath the surface ocean mixed layer relative to the subpolar gyre index (SPGI), as well as the NAOI. At the sea surface, direct relationships between the NAOI and hydrographic properties might be expected [*Thomas et al.*, 2008; *Reverdin*, 2010], as the NAOI is defined in terms of atmospheric conditions [*Hurrell et al.*, 2003]. Despite the ability of the NAO to influence the subpolar gyre, the relationship between the NAOI and SPGI is nonlinear and asymmetric (the response of the subpolar gyre to a negative NAOI phase is not simply the opposite of its response to a positive) [*Lohmann et al.*, 2008]. As an oceanic property, the SPGI is perhaps more likely than the NAOI to directly correlate with changes in DIC, even if the ultimate driver of those changes is the NAO.

4.3.4. Applicability of EEL Rates of Change to Wider Area

The TAA data set can be compared with FAA, in order to evaluate how changes observed at the EEL represent changes in the wider surrounding regions, in the model domain. This comparison suggests that changes observed in the EEL water column are representative of changes on a much larger spatial scale. However, the region that is most closely represented by the EEL varies with σ_0. For illustrative purposes, we take the mean value of ΔdDIC/dt (and its standard deviation) and its components ((1) through (4)) at each σ_0 level across all model stations in the FAA data set within the latitude range from 25 to 40°N and longitude range from 070 to 030°W to be representative of the North Atlantic and from 66 to 72°N and 012°W to 001°E equivalently for the Nordic Seas (Figure 7). Therefore, if the mean ΔdX/dt for any variable X in either region is close to 0, it means that the region's dX/dt is similar to that observed at the EEL, which is then considered to represent that region well. Positive ΔdX/dt indicates a faster increase (or slower decrease) in X at the station than at the EEL, and the opposite applies for negative values.

(a) $\sigma_0 = 27.25$ kg m^{-3}
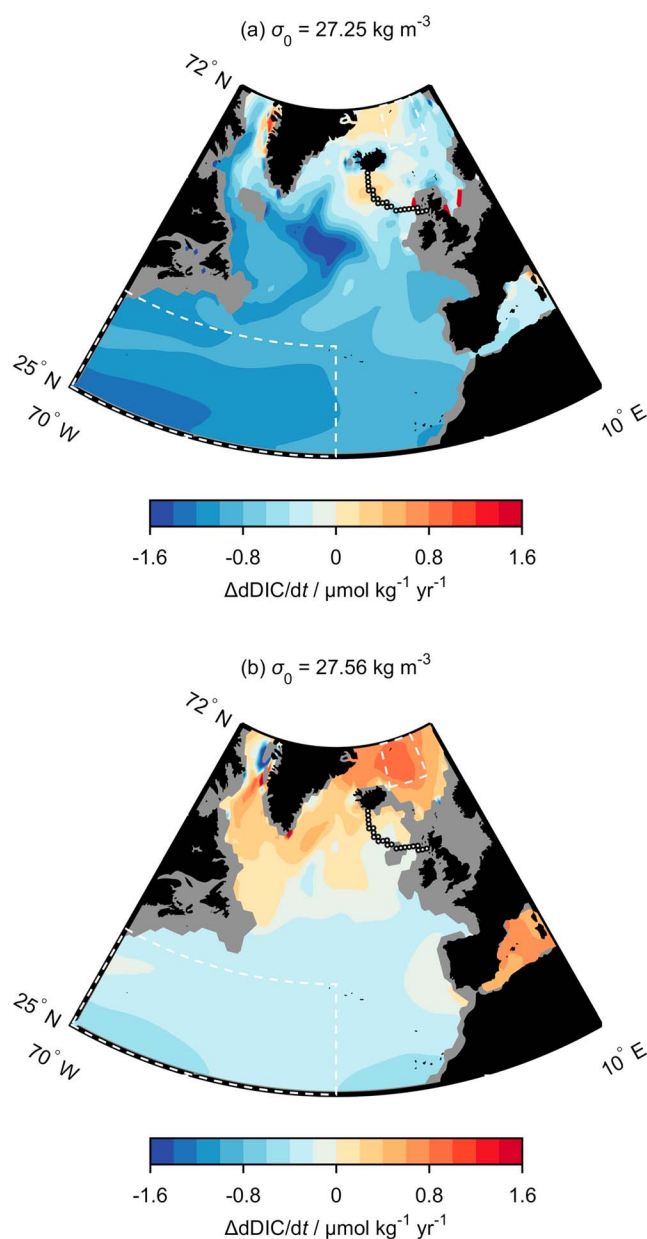

(b) $\sigma_0 = 27.56$ kg m^{-3}

Figure 8. Rate of change of DIC at each "station" in the FAA model data set relative to its value at the same σ_0 level in TAA, for (a) $\sigma_0 = 27.25$ kg m^{-3} and (b) $\sigma_0 = 27.56$ kg m^{-3}. Positive values (red) indicate higher dDIC/dt in situ compared with at the EEL (i.e., dDIC/dt is greater in FAA than in TAA), and negatives (blue) indicate the opposite. The black circles between Scotland and Iceland show the model stations representing idealized EEL (i.e., the TAA dataset). The white dashed lines near the northeast and southwest corners of the maps enclose the areas considered to represent the North Atlantic and Nordic Seas for Figure 7.

For most of the water column (σ_0 from 27.0 to 27.8 kg m^{-3}), dDIC/dt is between 0.5 and 1.5 μmol kg^{-1} yr^{-1} higher in the Nordic Seas than in the North Atlantic, but the position of the EEL on this gradient shifts with depth (Figure 7a). In the upper part of the water column ($\sigma_0 < 27.35$ kg m^{-3}, e.g., Figure 8a), ΔdDIC/dt is close to 0 for the Nordic Seas, but at higher σ_0 (e.g., Figure 8b) the EEL rate more closely resembles the North Atlantic. The divide between upper and lower water column in this context, at σ_0 between 27.3 and 27.4 kg m^{-3}, corresponds to a depth of roughly 300 to 500 m at the EEL and the bottom of the thermocline. Both the DIC$_{soft}$ (Figure 7b) and DIC$_{carb}$ (Figure 7c) components exhibit similar patterns as the total DIC change—that is, the EEL is changing more like the Nordic Seas in the upper water column and North Atlantic lower down. However, because of how these components are combined to calculate the anthropogenic contribution to DIC change (1), the pattern is reversed for DIC$_{anth}$. Its rate of accumulation in the upper water column is similar to the North Atlantic, while it matches the Nordic Seas at greater depths.

We can draw several conclusions from this part of the analysis. For a significant section of the water column, several variables are changing at the same rate at the EEL as they are throughout the wider surrounding regions in the model domain. However, different variables (and components of variables) at any given σ_0 level may not reflect changes in the same adjacent region as each other. It is reasonable to expect that the base of the thermocline might be the σ_0 range where the EEL switches from representing one adjacent region to the other, as that is where the main currents change between traveling to the north and to the south at the EEL [*Hansen and Østerhus*, 2000]. Our analysis indicates that changes in DIC and its components are sufficiently spatially coherent that measurements of their changes along the EEL are representative of similar basin-wide changes.

5. Conclusions

Sufficient measurements have now been made along the Extended Ellett Line (EEL) transect to establish a time series of data from which increases in DIC can be identified throughout the water column when

combined with historical data sets. Most of the increase in DIC occurs in and above the thermocline. Anthropogenic CO_2 accumulation has driven $31 \pm 6\%$ of the column inventory change in DIC, while the rest is due to increases in organic matter remineralization. The latter is likely driven by a net contraction of the North Atlantic subpolar gyre, and therefore an increasing influence of southern sourced waters, during the time period considered in this study. The isotopic data provide independent supporting evidence for the attribution of DIC changes to these different driving processes. We found that values of $-0.0166 \pm 0.0003‰$ $(\mu mol\, kg^{-1})^{-1}$ for ΔRC and $-27.0 \pm 0.5‰$ for $\delta^{13}C_{POC}$ were best able to explain the observed $d\delta^{13}C_{DIC}/dt$ profile.

Future EEL occupations will provide additional data to extend this time series analysis. Once more, consecutive years of data become available, it may also become possible to better assess the influence of processes operating on subdecadal timescales, for example, the North Atlantic Oscillation. A more robust quantification of interannual variability at the EEL will be useful to better evaluate the confidence bounds on rate of change calculations and times of emergence for long-term trends.

Combination of the observational data with output from model simulations demonstrated that the spatio-temporal heterogeneity in the distribution of the observations does not adversely affect the calculated rates of change. The model data have also provided insight into the relevance of the EEL in a larger regional setting, suggesting that changes observed locally may reflect much wider scale changes occurring in the North Atlantic Ocean and Nordic Seas.

References

Ahn, J., E. J. Brook, L. Mitchell, J. Rosen, J. R. McConnell, K. Taylor, D. Etheridge, and M. Rubino (2012), Atmospheric CO_2 over the last 1000 years: A high-resolution record from the West Antarctic Ice Sheet (WAIS) Divide ice core, *Global Biogeochem. Cycles*, *26*, GB2027, doi:10.1029/2011GB004247.

Anderson, L. A. (1995), On the hydrogen and oxygen content of marine phytoplankton, *Deep Sea Res., Part I*, *42*(9), 1675–1680, doi:10.1016/0967-0637(95)00072-E.

Anderson, L. A., and J. L. Sarmiento (1994), Redfield ratios of remineralization determined by nutrient data analysis, *Global Biogeochem. Cycles*, *8*(1), 65–80, doi:10.1029/93GB03318.

Barrier, N., C. Cassou, J. Deshayes, and A.-M. Treguier (2014), Response of North Atlantic Ocean circulation to atmospheric weather regimes, *J. Phys. Oceanogr.*, *44*(1), 179–201, doi:10.1175/JPO-D-12-0217.1.

Bates, N. R., M. H. P. Best, K. Neely, R. Garley, A. G. Dickson, and R. J. Johnson (2012), Detecting anthropogenic carbon dioxide uptake and ocean acidification in the North Atlantic Ocean, *Biogeosciences*, *9*(7), 2509–2522, doi:10.5194/bg-9-2509-2012.

Bates, N. R., Y. M. Astor, M. J. Church, K. Currie, J. E. Dore, M. González-Dávila, L. Lorenzoni, F. Muller-Karger, J. Olafsson, and J. M. Santana Casiano (2014), A time-series view of changing ocean chemistry due to ocean uptake of anthropogenic CO_2 and ocean acidification, *Oceanography*, *27*(1), 126–141, doi:10.5670/oceanog.2014.16.

Brewer, P. G. (1978), Direct observation of the oceanic CO_2 increase, *Geophys. Res. Lett.*, *5*(12), 997–1000, doi:10.1029/GL005i012p00997.

Brewer, P. G., J. L. Sarmiento, and W. M. Smethie (1985), The Transient Tracers in the Ocean (TTO) program: The North Atlantic study, 1981; The tropical atlantic study, 1983, *J. Geophys. Res.*, *90*(C4), 6903–6905, doi:10.1029/JC090iC04p06903.

Burkholder, K. C., and M. S. Lozier (2011), Mid-depth Lagrangian pathways in the North Atlantic and their impact on the salinity of the eastern subpolar gyre, *Deep Sea Res., Part I*, *58*(12), 1196–1204, doi:10.1016/j.dsr.2011.08.007.

Caldeira, K., and M. E. Wickett (2003), Anthropogenic carbon and ocean pH, *Nature*, *425*(6956), 365–365, doi:10.1038/425365a.

Chen, G.-T., and F. J. Millero (1979), Gradual increase of oceanic CO_2, *Nature*, *277*(5693), 205–206, doi:10.1038/277205a0.

Collins, W. J., et al. (2011), Development and evaluation of an Earth-System model—HadGEM2, *Geosci. Model Dev.*, *4*(4), 1051–1075, doi:10.5194/gmd-4-1051-2011.

Doney, S. C., V. J. Fabry, R. A. Feely, and J. A. Kleypas (2009), Ocean acidification: The other CO_2 problem, *Annu. Rev. Mar. Sci.*, *1*, 169–192, doi:10.1146/annurev.marine.010908.163834.

Dore, J. E., R. Lukas, D. W. Sadler, M. J. Church, and D. M. Karl (2009), Physical and biogeochemical modulation of ocean acidification in the central North Pacific, *Proc. Natl. Acad. Sci. U.S.A.*, *106*(30), 12,235–12,240, doi:10.1073/pnas.0906044106.

Dunne, J. P., J. L. Sarmiento, and A. Gnanadesikan (2007), A synthesis of global particle export from the surface ocean and cycling through the ocean interior and on the seafloor, *Global Biogeochem. Cycles*, *21*, GB4006, doi:10.1029/2006GB002907.

Eakins, B. W., and G. F. Sharman (2010), *Volumes of the World's Oceans From ETOPO1*, NOAA National Geophysical Data Cent., Boulder, Colo.

Friis, K., A. Körtzinger, J. Pätsch, and D. W. R. Wallace (2005), On the temporal increase of anthropogenic CO_2 in the subpolar North Atlantic, *Deep Sea Res., Part I*, *52*(5), 681–698, doi:10.1016/j.dsr.2004.11.017.

Fritsch, F., and R. Carlson (1980), Monotone piecewise cubic interpolation, *SIAM J. Numer. Anal.*, *17*(2), 238–246, doi:10.1137/0717021.

García, H. E., and L. I. Gordon (1992), Oxygen solubility in seawater: Better fitting equations, *Limnol. Oceanogr.*, *37*(6), 1307–1312, doi:10.4319/lo.1992.37.6.1307.

Gaylord, B., et al. (2015), Ocean acidification through the lens of ecological theory, *Ecology*, *96*(1), 3–15, doi:10.1890/14-0802.1.

Goericke, R., and B. Fry (1994), Variations of marine plankton $\delta^{13}C$ with latitude, temperature, and dissolved CO_2 in the world ocean, *Global Biogeochem. Cycles*, *8*(1), 85–90, doi:10.1029/93GB03272.

González-Dávila, M., J. M. Santana-Casiano, M. J. Rueda, and O. Llinás (2010), The water column distribution of carbonate system variables at the ESTOC site from 1995 to 2004, *Biogeosciences*, *7*(10), 3067–3081, doi:10.5194/bg-7-3067-2010.

Goodkin, N. F., N. M. Levine, S. C. Doney, and R. Wanninkhof (2011), Impacts of temporal CO_2 and climate trends on the detection of ocean anthropogenic CO_2 accumulation, *Global Biogeochem. Cycles*, *25*, GB3023, doi:10.1029/2010GB004009.

Gregg, W. W., and C. S. Rousseaux (2014), Decadal trends in global pelagic ocean chlorophyll: A new assessment integrating multiple satellites, in situ data, and models, *J. Geophys. Res. Oceans*, *119*, 5921–5933, doi:10.1002/2014JC010158.

Griffiths, C. R. (Ed) (2012), *RRS Discovery* Cruise D379, Southampton to Reykjavik, Extended Ellett Line, pp. 184, Scot. Association for Marine Science, Oban, UK.

Griffiths, C. R., and N. P. Holliday (Eds) (2013), *RRS James Cook*, Cruise JC086: Glasgow to Glasgow, Extended Ellett Line, 6th May 2013 > 26th May 2013, pp. 229, Scot. Association for Marine Science, Oban, U. K.

Gruber, N. (2009), Carbon cycle: Fickle trends in the ocean, *Nature*, *458*(7235), 155–156, doi:10.1038/458155a.

Gruber, N., J. L. Sarmiento, and T. F. Stocker (1996), An improved method for detecting anthropogenic CO_2 in the oceans, *Global Biogeochem. Cycles*, *10*(4), 809–837, doi:10.1029/96GB01608.

Gruber, N., C. D. Keeling, R. B. Bacastow, P. R. Guenther, T. J. Lueker, M. Wahlen, H. A. J. Meijer, W. G. Mook, and T. F. Stocker (1999), Spatiotemporal patterns of carbon-13 in the global surface oceans and the oceanic Suess effect, *Global Biogeochem. Cycles*, *13*(2), 307–335, doi:10.1029/1999GB900019.

Häkkinen, S., and P. B. Rhines (2004), Decline of subpolar North Atlantic circulation during the 1990s, *Science*, *304*(5670), 555–559, doi:10.1126/science.1094917.

Hansen, B., and S. Østerhus (2000), North Atlantic–Nordic Seas exchanges, *Prog. Oceanogr.*, *45*(2), 109–208, doi:10.1016/S0079-6611(99)00052-X.

Hátún, H., A. B. Sandø, H. Drange, B. Hansen, and H. Valdimarsson (2005), Influence of the Atlantic subpolar gyre on the thermohaline circulation, *Science*, *309*(5742), 1841–1844, doi:10.1126/science.1114777.

Heimann, M., and E. Maier-Reimer (1996), On the relations between the oceanic uptake of CO_2 and its carbon isotopes, *Global Biogeochem. Cycles*, *10*(1), 89–110, doi:10.1029/95GB03191.

Henson, S. A., R. Sanders, and E. Madsen (2012), Global patterns in efficiency of particulate organic carbon export and transfer to the deep ocean, *Global Biogeochem. Cycles*, *26*, GB1028, doi:10.1029/2011GB004099.

Heuzé, C., K. J. Heywood, D. P. Stevens, and J. K. Ridley (2013), Southern Ocean bottom water characteristics in CMIP5 models, *Geophys. Res. Lett.*, *40*, 1409–1414, doi:10.1002/grl.50287.

Heuzé, C., K. J. Heywood, D. P. Stevens, and J. K. Ridley (2014), Changes in global ocean bottom properties and volume transports in CMIP5 models under climate change scenarios, *J. Clim.*, doi:10.1175/JCLI-D-14-00381.1.

Hieronymus, M., and J. Nycander (2013), The budgets of heat and salinity in NEMO, *Ocean Model.*, *67*, 28–38, doi:10.1016/j.ocemod.2013.03.006.

Holliday, N. P., and S. Cunningham (2013), The Extended Ellett Line: Discoveries from 65 years of marine observations west of the U. K., *Oceanography*, *26*(2), 156–163, doi:10.5670/oceanog.2013.17.

Hughes, S. L., N. P. Holliday, and F. Gaillard (2012), Variability in the ICES/NAFO region between 1950 and 2009: Observations from the ICES Report on Ocean Climate, *ICES J. Mar. Sci.*, *69*(5), 706–719, doi:10.1093/icesjms/fss044.

Humphreys, M. P., E. P. Achterberg, A. M. Griffiths, A. McDonald, and A. J. Boyce (2015), Measurements of the stable carbon isotope composition of dissolved inorganic carbon in the northeastern Atlantic and Nordic Seas during summer 2012, *Earth Syst. Sci. Data*, *7*, 127–135, doi:10.5194/essd-7-127-2015.

Hurrell, J. W., Y. Kushnir, G. Ottersen, and M. Visbeck (2003), An overview of the North Atlantic Oscillation, in *The North Atlantic Oscillation: Climatic Significance and Environmental Impact*, pp. 1–35, AGU, Washington, D. C.

International Panel on Climate Change (2013), *Climate Change 2013: The Physical Science Basis. Contribution of Working Group I to the Fifth Assessment Report of the Intergovernmental Panel on Climate Change*, edited by T. F. Stocker et al., Cambridge Univ. Press, Cambridge, U. K. and New York.

Jeansson, E., A. Olsen, T. Eldevik, I. Skjelvan, A. M. Omar, S. K. Lauvset, J. E. Ø. Nilsen, R. G. J. Bellerby, T. Johannessen, and E. Falck (2011), The Nordic Seas carbon budget: Sources, sinks, and uncertainties, *Global Biogeochem. Cycles*, *25*, GB4010, doi:10.1029/2010GB003961.

Johnson, C., M. Inall, and S. Häkkinen (2013), Declining nutrient concentrations in the northeast Atlantic as a result of a weakening Subpolar Gyre, *Deep Sea Res., Part I*, *82*, 95–107, doi:10.1016/j.dsr.2013.08.007.

Jutterström, S., E. Jeansson, L. G. Anderson, R. Bellerby, E. P. Jones, W. M. Smethie Jr., and J. H. Swift (2008), Evaluation of anthropogenic carbon in the Nordic Seas using observed relationships of N, P and C versus CFCs, *Prog. Oceanogr.*, *78*(1), 78–84, doi:10.1016/j.pocean.2007.06.001.

Kahaner, D., C. Moler, and S. Nash (1988), *Numerical Methods and Software*, Prentice Hall, Englewood Cliffs, N. J.

Keeling, C. D. (1979), The Suess effect: [13]Carbon-[14]carbon interrelations, *Environ. Int.*, *2*(4–6), 229–300, doi:10.1016/0160-4120(79)90005-9.

Key, R. M., A. Kozyr, C. L. Sabine, K. Lee, R. Wanninkhof, J. L. Bullister, R. A. Feely, F. J. Millero, C. Mordy, and T.-H. Peng (2004), A global ocean carbon climatology: Results from Global Data Analysis Project (GLODAP), *Global Biogeochem. Cycles*, *18*, GB4031, doi:10.1029/2004GB002247.

Key, R. M., et al. (2010), The CARINA data synthesis project: Introduction and overview, *Earth Syst. Sci. Data*, *2*(1), 105–121, doi:10.5194/essd-2-105-2010.

Khatiwala, S., F. Primeau, and T. Hall (2009), Reconstruction of the history of anthropogenic CO_2 concentrations in the ocean, *Nature*, *462*(7271), 346–349, doi:10.1038/nature08526.

Khatiwala, S., et al. (2013), Global ocean storage of anthropogenic carbon, *Biogeosciences*, *10*(4), 2169–2191, doi:10.5194/bg-10-2169-2013.

Kieke, D., M. Rhein, L. Stramma, W. M. Smethie, J. L. Bullister, and D. A. LeBel (2007), Changes in the pool of Labrador Sea Water in the subpolar North Atlantic, *Geophys. Res. Lett.*, *34*, L06605, doi:10.1029/2006GL028959.

Körtzinger, A., P. D. Quay, and R. E. Sonnerup (2003), Relationship between anthropogenic CO_2 and the [13]C Suess effect in the North Atlantic Ocean, *Global Biogeochem. Cycles*, *17*(1, 1005), doi:10.1029/2001GB001427.

Le Quéré, C., et al. (2009), Trends in the sources and sinks of carbon dioxide, *Nat. Geosci.*, *2*(12), 831–836, doi:10.1038/ngeo689.

Le Quéré, C., T. Takahashi, E. T. Buitenhuis, C. Rödenbeck, and S. C. Sutherland (2010), Impact of climate change and variability on the global oceanic sink of CO_2, *Global Biogeochem. Cycles*, *24*, GB4007, doi:10.1029/2009GB003599.

Lee, K., T.-W. Kim, R. H. Byrne, F. J. Millero, R. A. Feely, and Y.-M. Liu (2010), The universal ratio of boron to chlorinity for the North Pacific and North Atlantic oceans, *Geochim. Cosmochim. Acta*, *74*(6), 1801–1811, doi:10.1016/j.gca.2009.12.027.

Lohmann, K., H. Drange, and M. Bentsen (2008), Response of the North Atlantic subpolar gyre to persistent North Atlantic oscillation like forcing, *Clim. Dyn.*, *32*(2-3), 273–285, doi:10.1007/s00382-008-0467-6.

Lueker, T. J., A. G. Dickson, and C. D. Keeling (2000), Ocean pCO$_2$ calculated from dissolved inorganic carbon, alkalinity, and equations for K_1 and K_2: Validation based on laboratory measurements of CO_2 in gas and seawater at equilibrium, *Mar. Chem.*, *70*(1–3), 105–119, doi:10.1016/S0304-4203(00)00022-0.

Lynch-Stieglitz, J., T. F. Stocker, W. S. Broecker, and R. G. Fairbanks (1995), The influence of air-sea exchange on the isotopic composition of oceanic carbon: Observations and modeling, *Global Biogeochem. Cycles*, *9*(4), 653–666, doi:10.1029/95GB02574.

Madec, G. (2008), NEMO reference manual, ocean dynamic component: NEMO–OPA, Note du Pôle de modélisation, Institut Pierre Simon Laplace, France, Technical Report 27.

Matsumoto, K., and N. Gruber (2005), How accurate is the estimation of anthropogenic carbon in the ocean? An evaluation of the ΔC* method, *Global Biogeochem. Cycles*, *19*, GB3014, doi:10.1029/2004GB002397.

McDougall, T. J., and P. M. Barker (2011), Getting started with TEOS-10 and the Gibbs Seawater (GSW) oceanographic toolbox, SCOR/IAPSO WG127.

McGrath, T., G. Nolan, and E. McGovern (2012a), Chemical characteristics of water masses in the Rockall Trough, *Deep Sea Res., Part I*, *61*, 57–73, doi:10.1016/j.dsr.2011.11.007.

McGrath, T., C. Kivimäe, T. Tanhua, R. R. Cave, and E. McGovern (2012b), Inorganic carbon and pH levels in the Rockall Trough 1991–2010, *Deep Sea Res., Part I*, *68*, 79–91, doi:10.1016/j.dsr.2012.05.011.

McNeil, B. I., R. J. Matear, and B. Tilbrook (2001), Does carbon 13 track anthropogenic CO_2 in the Southern Ocean?, *Global Biogeochem. Cycles*, *15*(3), 597–613, doi:10.1029/2000GB001352.

Olafsson, J., S. R. Olafsdottir, A. Benoit-Cattin, M. Danielsen, T. S. Arnarson, and T. Takahashi (2009), Rate of Iceland Sea acidification from time series measurements, *Biogeosciences*, *6*(11), 2661–2668, doi:10.5194/bg-6-2661-2009.

Olsen, A., and U. Ninnemann (2010), Large δ^{13}C gradients in the preindustrial North Atlantic revealed, *Science*, *330*(6004), 658–659, doi:10.1126/science.1193769.

Olsen, A., et al. (2006), Magnitude and origin of the anthropogenic CO_2 increase and ^{13}C Suess effect in the Nordic seas since 1981, *Global Biogeochem. Cycles*, *20*, GB3027, doi:10.1029/2005GB002669.

Olsen, A., A. M. Omar, E. Jeansson, L. G. Anderson, and R. G. J. Bellerby (2010), Nordic seas transit time distributions and anthropogenic CO_2, *J. Geophys. Res.*, *115*, C05005, doi:10.1029/2009JC005488.

Pérez, F. F., M. Vázquez-Rodríguez, H. Mercier, A. Velo, P. Lherminier, and A. F. Ríos (2010), Trends of anthropogenic CO_2 storage in North Atlantic water masses, *Biogeosciences*, *7*(5), 1789–1807, doi:10.5194/bg-7-1789-2010.

Quay, P. D., R. Sonnerup, J. Stutsman, J. Maurer, A. Körtzinger, X. A. Padin, and C. Robinson (2007), Anthropogenic CO_2 accumulation rates in the North Atlantic Ocean from changes in the ^{13}C/^{12}C of dissolved inorganic carbon, *Global Biogeochem. Cycles*, *21*, GB1009, doi:10.1029/2006GB002761.

Rau, G. H., U. Riebesell, and D. Wolf-Gladrow (1997), CO_{2aq}-dependent photosynthetic ^{13}C fractionation in the ocean: A model versus measurements, *Global Biogeochem. Cycles*, *11*(2), 267–278, doi:10.1029/97GB00328.

Read, J. F. (2010), *RRS Discovery* Cruise 351: 10-28 May 2010, The Extended Ellett Line 2010, pp. 117, National Oceanography Centre, Southampton, U. K.

Read, J. F. (2011), *RRS Discovery* Cruise 365: 11 May-02 Jun 2011, The Extended Ellett Line 2011, pp. 90, National Oceanography Centre, Southampton, U. K.

Redfield, A. C., B. H. Ketchum, and F. A. Richards (1963), The influence of organisms on the composition of sea-water, in *The Sea*, vol. 2, pp. 26–77, Interscience, New York.

Reverdin, G. (2010), North Atlantic Subpolar Gyre Surface Variability (1895–2009), *J, Climate*, *23*(17), 4571–4584, doi:10.1175/2010JCLI3493.1.

Riahi, K., S. Rao, V. Krey, C. Cho, V. Chirkov, G. Fischer, G. Kindermann, N. Nakicenovic, and P. Rafaj (2011), RCP 8.5—A scenario of comparatively high greenhouse gas emissions, *Clim. Change*, *109*(1–2), 33–57, doi:10.1007/s10584-011-0149-y.

Romanek, C. S., E. L. Grossman, and J. W. Morse (1992), Carbon isotopic fractionation in synthetic aragonite and calcite: Effects of temperature and precipitation rate, *Geochim. Cosmochim. Acta*, *56*(1), 419–430, doi:10.1016/0016-7037(92)90142-6.

Sabine, C. L., and T. Tanhua (2010), Estimation of anthropogenic CO_2 inventories in the ocean, *Annu. Rev. Mar. Sci.*, *2*, 175–198, doi:10.1146/annurev-marine-120308-080947.

Sabine, C. L., et al. (2004), The oceanic sink for anthropogenic CO_2, *Science*, *305*(5682), 367–371, doi:10.1126/science.1097403.

Schmittner, A., N. Gruber, A. C. Mix, R. M. Key, A. Tagliabue, and T. K. Westberry (2013), Biology and air–sea gas exchange controls on the distribution of carbon isotope ratios (δ^{13}C) in the ocean, *Biogeosciences*, *10*(9), 5793–5816, doi:10.5194/bg-10-5793-2013.

Schuster, U., A. J. Watson, N. R. Bates, A. Corbière, M. González-Dávila, N. Metzl, D. Pierrot, and M. Santana-Casiano (2009), Trends in North Atlantic sea-surface fCO_2 from 1990 to 2006, *Deep Sea Res., Part II*, *56*(8–10), 620–629, doi:10.1016/j.dsr2.2008.12.011.

Sherwin, T. (2009), *RRS Discovery*, Cruise D340a: Reykjavik to Dunstaffnage Via Rockall and the Wyville Thomson Ridge, 10 June to 25 June 2009, pp. 196, Scot. Association for Marine Science, Oban, U. K.

Steinfeldt, R., M. Rhein, J. L. Bullister, and T. Tanhua (2009), Inventory changes in anthropogenic carbon from 1997–2003 in the Atlantic Ocean between 20°S and 65°N, *Global Biogeochem. Cycles*, *23*, GB3010, doi:10.1029/2008GB003311.

Stendardo, I., D. Kieke, M. Rhein, N. Gruber, and R. Steinfeldt (2015), Interannual to decadal oxygen variability in the mid-depth water masses of the eastern North Atlantic, *Deep Sea Res., Part I*, *95*, 85–98, doi:10.1016/j.dsr.2014.10.009.

Tanhua, T., and D. W. R. Wallace (2005), Consistency of TTO-NAS inorganic carbon data with modern measurements, *Geophys. Res. Lett.*, *32*, L14618, doi:10.1029/2005GL023248.

Tanhua, T., A. Körtzinger, K. Friis, D. W. Waugh, and D. W. R. Wallace (2007), An estimate of anthropogenic CO_2 inventory from decadal changes in oceanic carbon content, *Proc. Natl. Acad. Sci. U.S.A.*, *104*(9), 3037–3042, doi:10.1073/pnas.0606574104.

Thomas, H., A. E. F. Prowe, I. D. Lima, S. C. Doney, R. Wanninkhof, R. J. Greatbatch, U. Schuster, and A. Corbière (2008), Changes in the North Atlantic Oscillation influence CO2 uptake in the North Atlantic over the past 2 decades, *Global Biogeochem. Cycles*, *22*, GB4027, doi:10.1029/2007GB003167.

Tjiputra, J. F., A. Olsen, L. Bopp, A. Lenton, B. Pfeil, T. Roy, J. Segschneider, I. Totterdell, and C. Heinze (2014), Long-term surface pCO_2 trends from observations and models, *Tellus B*, *66*, 23083, doi:10.3402/tellusb.v66.23083.

van Heuven, S., D. Pierrot, J. W. B. Rae, E. Lewis, and D. W. R. Wallace (2011), CO2SYS v 1.1, MATLAB program developed for CO_2 system calculations, *ORNL/CDIAC-105b. Carbon Dioxide Information Analysis Center, Oak Ridge National Laboratory, U.S. Department of Energy, Oak Ridge, Tenn*.

Wanninkhof, R., S. C. Doney, J. L. Bullister, N. M. Levine, M. Warner, and N. Gruber (2010), Detecting anthropogenic CO_2 changes in the interior Atlantic Ocean between 1989 and 2005, *J. Geophys. Res.*, *115*, C11028, doi:10.1029/2010JC006251.

Wolf-Gladrow, D. A., R. E. Zeebe, C. Klaas, A. Körtzinger, and A. G. Dickson (2007), Total alkalinity: The explicit conservative expression and its application to biogeochemical processes, *Mar. Chem.*, *106*(1–2), 287–300, doi:10.1016/j.marchem.2007.01.006.

Yashayaev, I., H. M. van Aken, N. P. Holliday, and M. Bersch (2007), Transformation of the Labrador Sea Water in the subpolar North Atlantic, *Geophys. Res. Lett.*, *34*, L22605, doi:10.1029/2007GL031812.

Yool, A., E. E. Popova, A. C. Coward, D. Bernie, and T. R. Anderson (2013a), Climate change and ocean acidification impacts on lower trophic levels and the export of organic carbon to the deep ocean, *Biogeosciences*, *10*(9), 5831–5854, doi:10.5194/bg-10-5831-2013.

Yool, A., E. E. Popova, and T. R. Anderson (2013b), MEDUSA-2.0: An intermediate complexity biogeochemical model of the marine carbon cycle for climate change and ocean acidification studies, *Geosci. Model Dev.*, *6*(5), 1767–1811, doi:10.5194/gmd-6-1767-2013.

Young, J. N., J. Bruggeman, R. E. M. Rickaby, J. Erez, and M. Conte (2013), Evidence for changes in carbon isotopic fractionation by phytoplankton between 1960 and 2010, *Global Biogeochem. Cycles*, *27*, 505–515, doi:10.1002/gbc.20045.